

Fermi National Accelerator Laboratory

FERMILAB-TM-1915

**The E760 Jet Target:  
Measurements of Performance at 77K**

G. Boero, M. Macri and E. Robutti

*I.N.F.N. e Dipartimento di Fisica dell'Universita di Genova  
Genoa, Italy*

D. Allspach, C. Kendziora and M. Marinelli

*Fermi National Accelerator Laboratory  
P.O. Box 500, Batavia, Illinois 60510*

November 1994

## **Disclaimer**

*This report was prepared as an account of work sponsored by an agency of the United States Government. Neither the United States Government nor any agency thereof, nor any of their employees, makes any warranty, express or implied, or assumes any legal liability or responsibility for the accuracy, completeness, or usefulness of any information, apparatus, product, or process disclosed, or represents that its use would not infringe privately owned rights. Reference herein to any specific commercial product, process, or service by trade name, trademark, manufacturer, or otherwise, does not necessarily constitute or imply its endorsement, recommendation, or favoring by the United States Government or any agency thereof. The views and opinions of authors expressed herein do not necessarily state or reflect those of the United States Government or any agency thereof.*

# THE E760 JET TARGET: MEASUREMENTS OF PERFORMANCE at 77K

*G. Boero, M. Macrì, E. Robutti*  
I.N.F.N. e Dipartimento di Fisica dell'Università di Genova

*D. Allspach, C. Kendziora, M. Marinelli\**  
Mechanical Support Department,  
Research Division  
Fermi National Accelerator Laboratory, Batavia, IL

## • Introduction

In this report we describe the measurements performed on the E760 hydrogen Jet Target in order to investigate some of the basic parameters of the system. These measurements were performed in the context of the upgrade program of the target for the successor experiment E835.

Fermilab experiment E760 studied charmonium states formed in antiproton-proton annihilations [1,2]. The antiproton-proton interactions were produced in a jet of hydrogen gas which intersected the antiproton beam coasting in the Fermilab Antiproton Accumulator.

The results from E760 have shown that an increase in integrated luminosity by a factor of more than 5 is needed to complete the study of the charmonium spectrum. The E835 experiment is designed to achieve this by increasing the intensity of the antiproton beam and the density of the hydrogen-cluster-jet. This report is concerned with preparations for the work needed to increase the density of the hydrogen-cluster-jet.

Figure 1 shows the geometry of the Hydrogen gas-jet and the antiproton beam and defines our coordinate system.

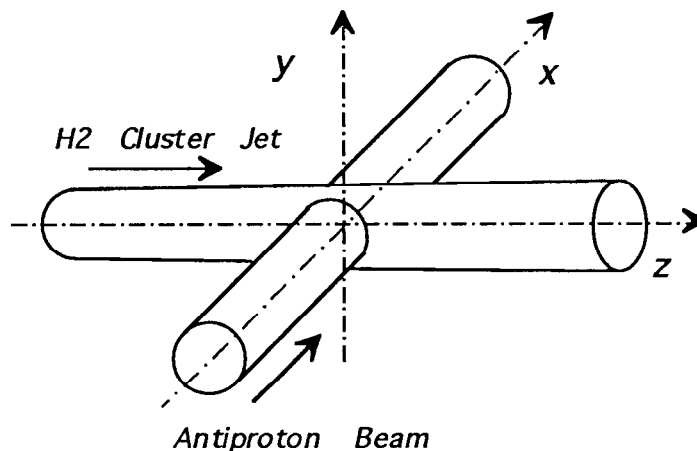


Fig.1. The antiproton beam-hydrogen cluster-jet interaction area.

---

\* Permanent address: Dipartimento di Fisica and I.N.F.N. -Via Dodecaneso 33 -16.146 Genoa (Italy)

The average density (atoms/cm<sup>3</sup>) of the cluster-jet is given by

$$\bar{\rho}_{\text{jet}} = \frac{\Phi_{\text{jet}}}{A_{\text{jet}} v_{\text{cl}}}, \quad (1)$$

where  $\Phi_{\text{jet}}$  is the cluster-jet flux (atoms/s),  $A_{\text{jet}}$  is the cluster-jet cross section in the interaction area and  $v_{\text{cl}}$  is the speed of the clusters. The experiment luminosity is directly proportional to the product of this density and the current of antiprotons; one wants therefore to maximize  $\Phi_{\text{jet}}$  and minimize  $v_{\text{cl}}$ . (Since the cluster-jet has cylindrical symmetry, the quantity  $A_{\text{jet}}$  is essentially set by the height of the antiproton beam and is not a free parameter). For reference, we show a schematic of the gas-jet target system as Figure 2, showing the various chambers the jet passes through and the associated pumping on each chamber. Figure 3 is a detail of the nozzle used to produce the jet of hydrogen cluster.  $P_0$  and  $T_0$  are the

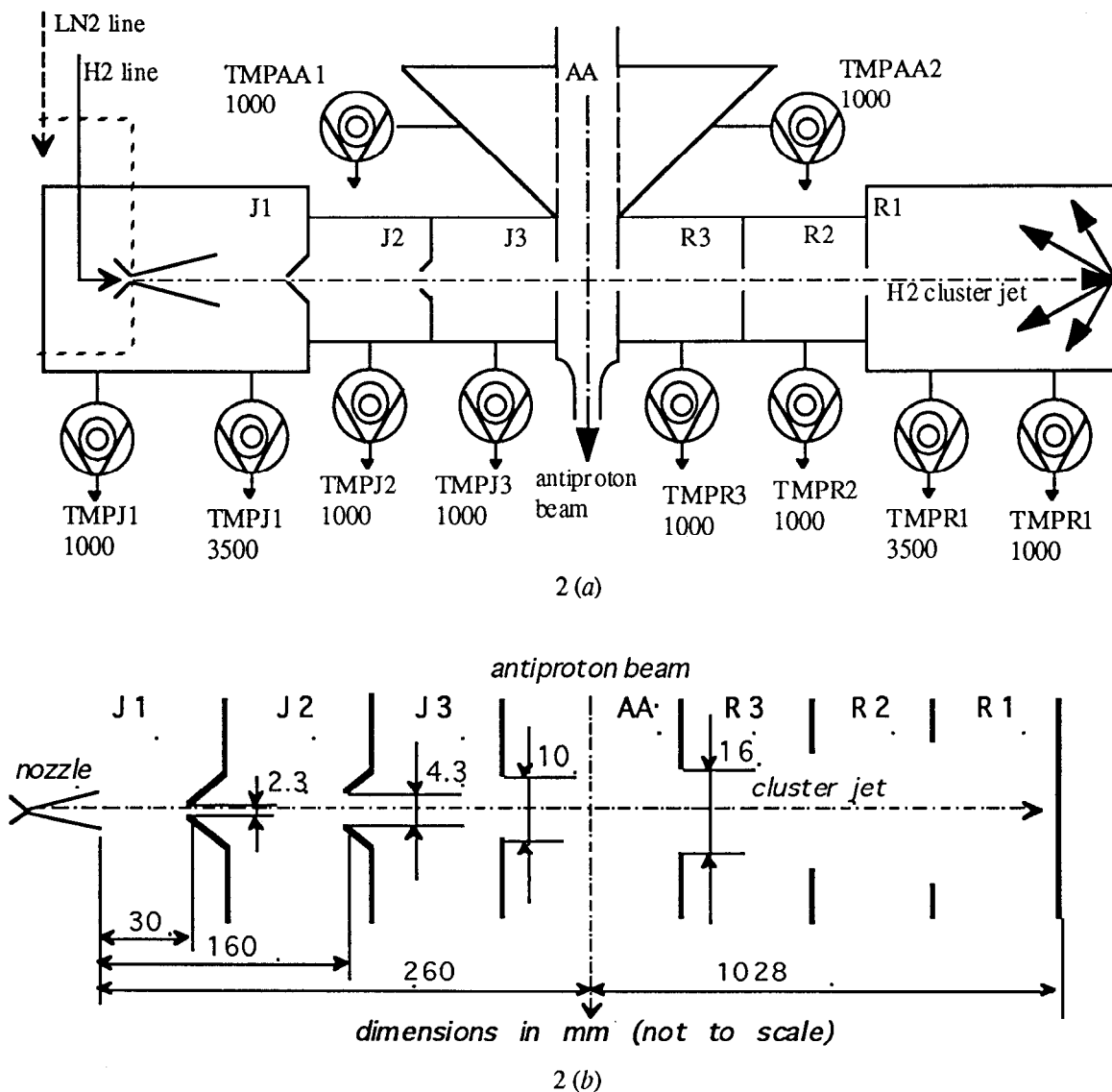


Fig.2. (a) Schematic of the Jet Target with the differential pumping stages: J1, J2, J3: (Jet) production stages; R1, R2, R3: (recovery) sink stages. (b) Pertinent Jet target dimensions.

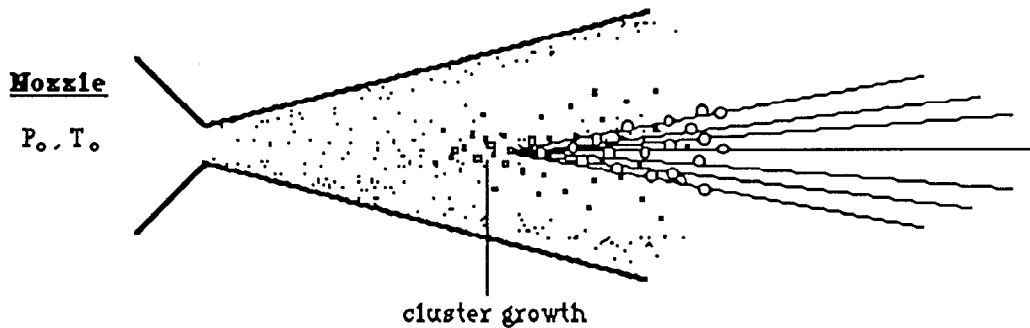


Fig.3. Condensation and formation of the cluster-jet during gas expansion inside the nozzle.

pressure in the hydrogen line and the temperature of the nozzle, respectively.

The Jet Target upgrade program includes:

a) Lowering the temperature (stagnation temperature  $T_0$ ) at which the hydrogen expansion begins from about 80 K to about 20 K. This will certainly decrease the clusters speed,  $v_{cl}$ , and perhaps produce some improvement in the cluster formation process thus increasing  $\Phi_{jet}$ .

b) Improving the pumping speed in the first chamber of the gas-jet system to reduce interaction between background gas in the chamber and the cluster-jet.

c) Control of the  $x$ - $y$  position of the nozzle and its angle (fig.1) to optimize transmission through the gas-jet collimator and skimmer system.

The work undertaken in the summer of 1993 was to build and test the apparatus and instrumentation to determine the important parameters of the gas-jet system performance prior to implementing the upgrades described above. The gas-jet target system was installed in the Proton Assembly Building at Fermilab and the following is a short report of the measurements at  $T_0=77$  K and their interpretation. The jet target density measured is in the range of  $10^{13}$  atoms/cm<sup>3</sup>. A complete report with a full description of our testing and results can be found in [4] and for the "nozzle physics" see [4,5,6]. These measurements have also given us new insights into the performance of the gas-jet system and we conclude with some suggestions about how to operate the gas-jet so as to maximize the luminosity of the experiment

- *Cluster-jet formation and nozzle mass flow*

Our cluster-jet is produced by letting hydrogen gas expand through a converging-diverging nozzle with a small diameter throat (20-100  $\mu$ m) and an opening angle of about 7 degrees (see figure 3). During the expansion [5,6] the H<sub>2</sub> molecules undergo a process of condensation which causes them to collect in clusters (in our case their size should be about  $10^4$ - $10^5$  atoms/cluster [7,8]). A jet of clusters is thus formed which constitutes the core of the hydrogen flow shown in fig. 3. To prevent uncondensed gas from diffusing into the Antiproton Accumulator beam-pipe, which would reduce the beam-lifetime without contributing to the experiment luminosity, the cluster-jet passes through a number of distinct chambers, connected by small holes or "skimmers". The defining aperture, or collimator, is the skimmer connecting the J2 and J3 chamber.

If we treat the expansion as an adiabatic process in a continuum flow regime, we can find an expression for the nozzle mass flow, assuming that the speed at the nozzle throat is equal to the local speed of sound at the stagnation condition (pressure  $P_0$  and temperature  $T_0$ ) and the nozzle geometry [5]:

$$\dot{m} = P_0 A_{th} \left[ \frac{\gamma W}{RT_0} \left( \frac{2}{\gamma + 1} \right)^{\frac{\gamma+1}{\gamma-1}} \right]^{\frac{1}{2}}, \quad (2)$$

where  $W$  is the gas molecular weight,  $A_{th}$  is the cross section of the nozzle throat and  $\gamma = c_p/c_v$  ( $\gamma = \frac{5}{3}$  for molecular hydrogen at low temperature). We have found this relation in good agreement with our experimental data at both liquid nitrogen temperature and room temperature using two different nozzles, both trumpet-shaped, with throat diameters of 37  $\mu\text{m}$  and 56  $\mu\text{m}$ .

- *Measurements of Cluster-jet flow and background gas*

The gas *throughput*  $Q$  (usually expressed in torr liter/sec) inside a chamber can be evaluated knowing the *pumping speed*  $S$  and the *pressure*  $P$  by means of the relation:

$$Q = SP. \quad (3)$$

The molecular flux (molecules/second) is then related to the throughput measured through the equation 1 torr-liter/sec =  $3.21 \cdot 10^{19}$  molecules/sec =  $6.42 \cdot 10^{19}$  atoms/sec, which applies at 300K, the temperature of the gas in the region of the ion gauges. Details of the calibration of the vacuum instruments used for the pressure measurement, a procedure which is especially important for the hot filament ionization gauges, are in reference [4]. We obtained the pumping speed on each of the jet target chambers by introducing a calibrated hydrogen leak flow (i.e. of known throughput) inside each chamber and measuring the subsequent pressure increase. The values found for the J1 chamber are plotted in fig. 5 as a function of the pressure in the chamber and show the typical behavior of constant pumping speed up to a pressure of a few  $10^{-2}$  torr. In table 1 we report all the measured pumping speeds and conductances. We have verified that the method used to introduce the calibrated leak into any chamber allows us to assume that the pressure increment produced at the pressure gauge for a given flow rate (number of atoms per unit time) into the chamber is the same whether the hydrogen is introduced through the calibrated leak or with the cluster-jet stream.

The "background" gas throughput is calculated from the pressure in the Antiproton Accumulator and the measured pumping speed  $S_{AA}$ .

- *Dependence of the gas jet throughput on pressure*

To determine the throughput into R1 we multiply the pressure increment inside the R1 chamber i.e. the pressure difference with the hydrogen jet on and off, by the R1 pumping speed. This is shown in fig.6a for two nozzle aperture sizes. Once the "clusterization" begins, the cluster-jet throughput grows almost linearly with the stagnation pressure. This clusterization begins at a lower pressure for the 56  $\mu\text{m}$  nozzle than for the 37  $\mu\text{m}$  nozzle (see also [6]). As the  $H_2$  line pressure increases, the R1 throughput

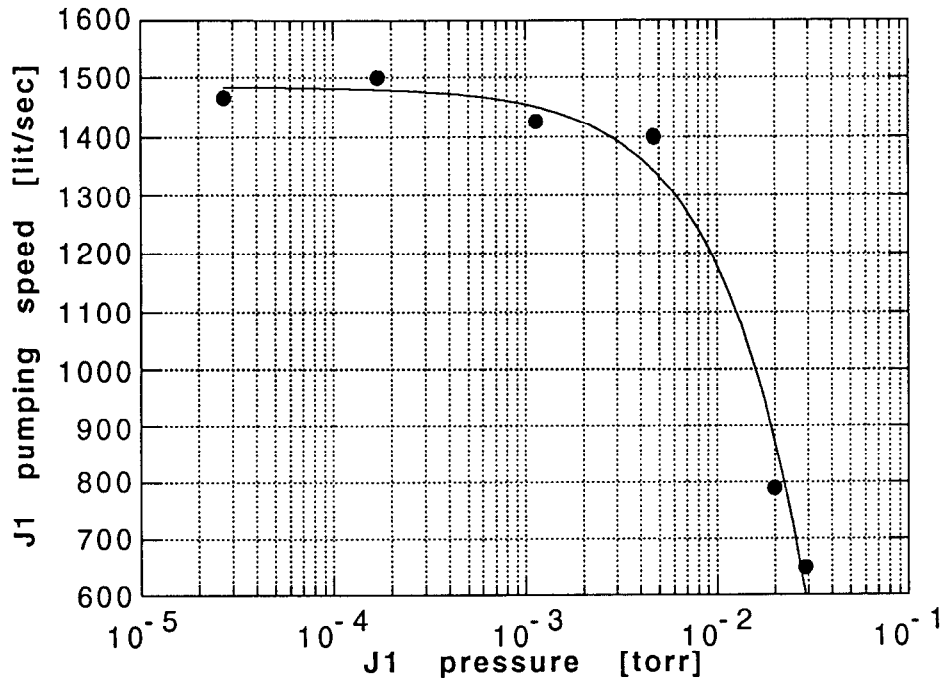


Fig.5. Measured pumping speed in J1 chamber as a function of the J1 pressure.

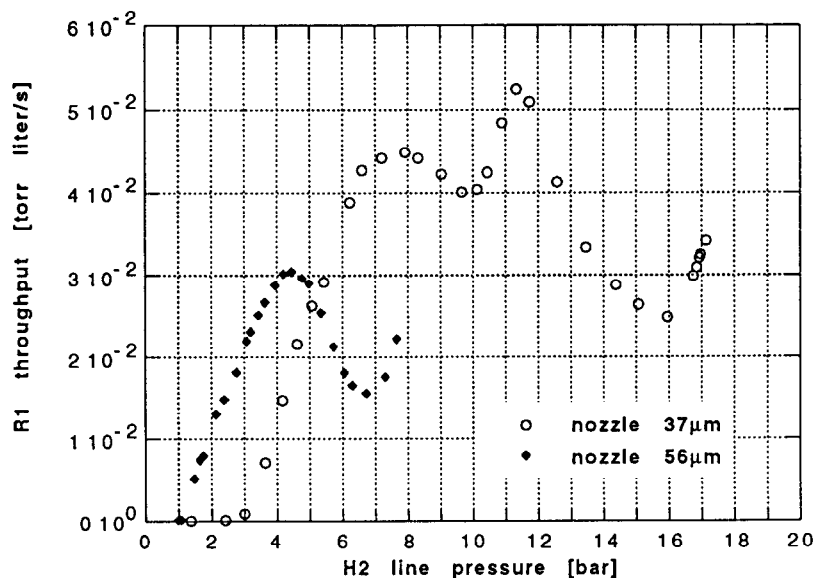
passes through a maximum value (the 37  $\mu\text{m}$  nozzle has two peaks which are not yet fully understood) and then decreases. For both nozzles we note that the throughput begins to decrease when the pressure in the J1 chamber reaches approximately  $10^{-2}$  torr. A reasonable explanation is that the amount of background gas at this pressure inhibits formation of any jet of  $\text{H}_2$  clusters.

Fig.6a also shows a second region where the throughput increases with pressure - at about 6.7 bar for the 56  $\mu\text{m}$  nozzle and at about 16 bar for the 37  $\mu\text{m}$  nozzle. At these high  $\text{H}_2$  line pressures we measured almost the same pressure in R1 when the jet was sent to the R1 chamber as when a metal plate was put in the Antiproton Accumulator pipe directly in the path of the jet. This implies that the throughput into R1 at higher pressures is due to diffusion of gas. The difference between the two throughput values (with the plate out of the beam and the plate in the beam) is shown in fig.6b. This quantity is taken as the cluster-jet throughput and is used in evaluating the cluster-jet density (eq.1).

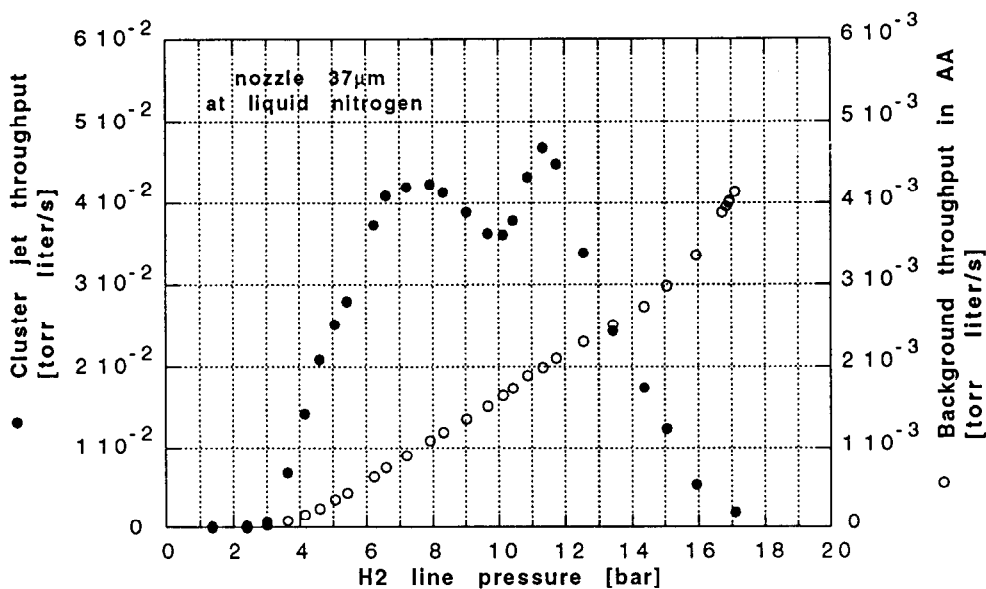
- *Measurements of the transverse density distribution of the jet.*

We used a simple method to find the shape of the jet at the interaction region, from which we obtain the jet cross section which appears in (1). The method makes use of a thin needle which can travel across the jet. This is similar to the technique originally used in the E760 set-up except that the needle location is now inside the Antiproton Accumulator pipe instead of in the R1 chamber as in E760. This technique is based on the principle that when the hydrogen clusters hit the needle, they break, or "evaporate", scattering individual molecules all around the chamber and causing an increase in pressure. The higher the rate of cluster hits, the larger the pressure rise.

To determine the jet shape we need to sweep its cross section in both the  $x$  and  $y$  (orthogonal) directions. To accomplish this we fixed an L-shaped needle of 0.85 mm diameter (fig.7) at the end of a long arm inserted in the Antiproton Accumulator pipe, perpendicular to the jet. The head supporting the needle is equipped with two kinds of movement each controlled with a stepping motor; the head can be moved back and forth along the  $x$  axis (thus allowing for horizontal sweep of the vertical part of the



6 (a)



6 (b)

Fig.6.(a) The throughput in R1 for nozzles with two different throat diameters. (b) The cluster-jet throughput and the background (see text) throughput into the Antiproton Accumulator for the 37  $\mu\text{m}$  nozzle.

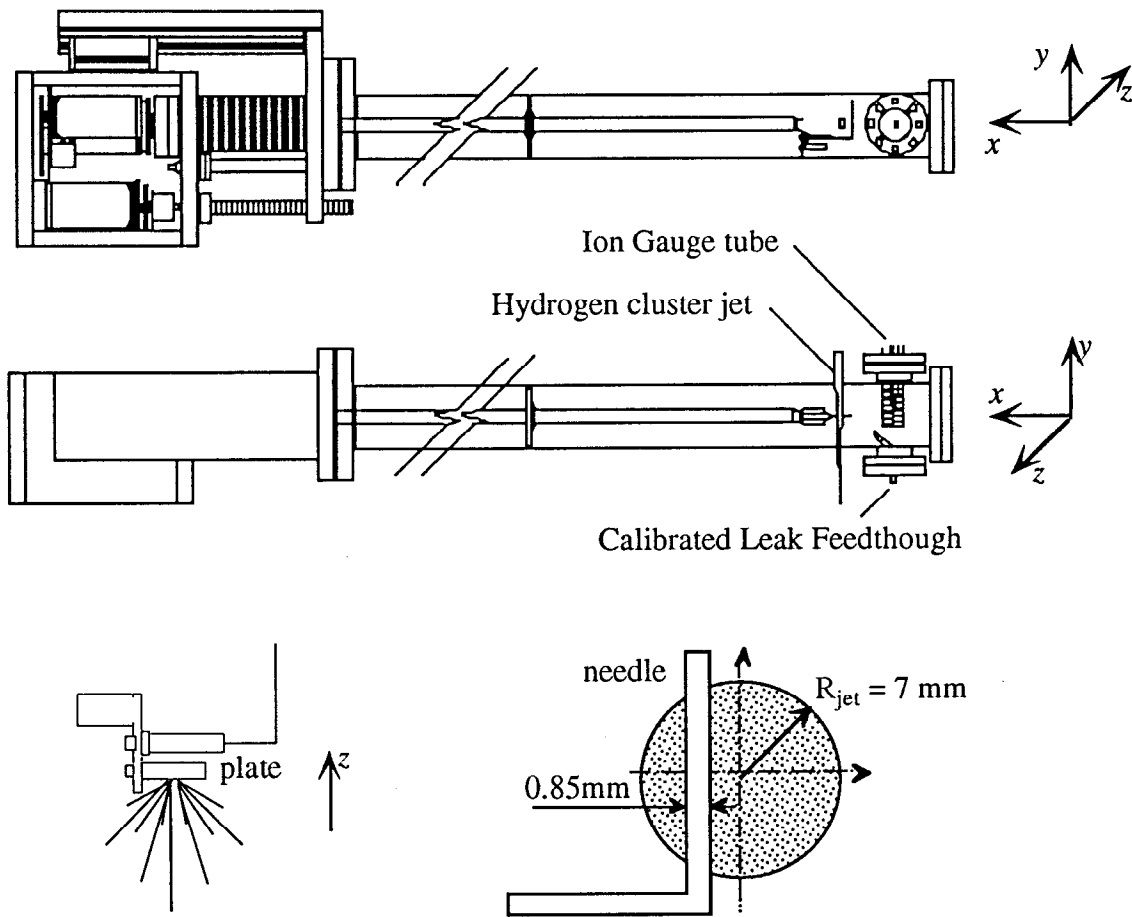
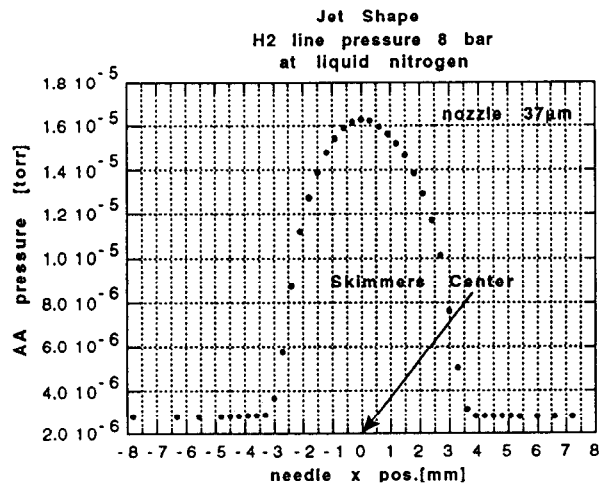


Fig.7. The *density detector*, used for measuring the geometry and throughput of the cluster-jet.

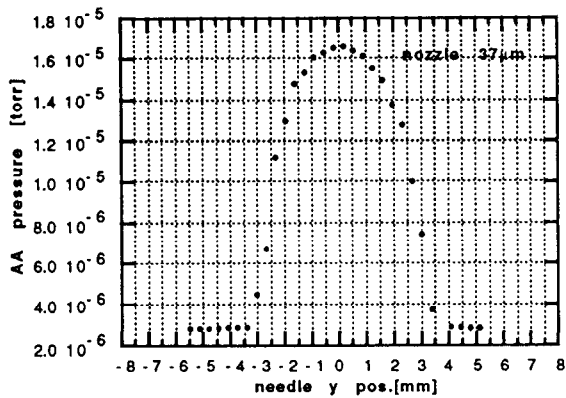
needle) and it can rotate around the  $x$  axis (thus allowing for a vertical sweep by the horizontal part of the needle).

The alignment of the entire system was verified by checking that the nozzle was located exactly on the  $z$  axis (machine axis, defined by the skimmer and collimator centers). We could do this directly by means of a small glass window inserted in the R1 wall in line with the nozzle, a telescope and a small light source placed inside the J1 chamber, thus lighting the nozzle exit.

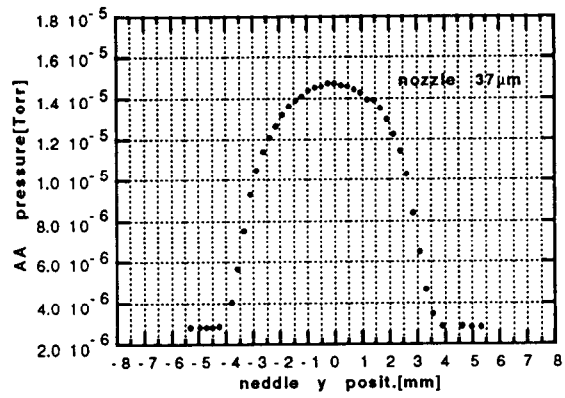
Measurements were made at several stagnation pressures and temperatures and with two nozzle throat diameters. We found that the geometric characteristics of the jet are independent of these parameters, being defined only by the collimator dimension and position with respect to the nozzle. A sample set of data is shown in figure 8. There are two different plots for the  $y$ -sweep because the needle crosses the jet at two different  $z$ -values (see fig.9). The main results of these measurements are: the jet is centered on the  $x$  axis to within about 0.5 mm, has a diameter of  $(7.0 \pm 0.5)$  mm, shows approximately cylindrical symmetry and does not have significant tails (1 mm inside its perimeter the density is more than 80% its maximum).



8 (a)



8 (b)



8 (c)

Fig.8. Jet shape plots: a) horizontal sweep; b) vertical sweep with needle at  $z = -19$  mm; c) vertical sweep with needle at  $z = +19$  mm.

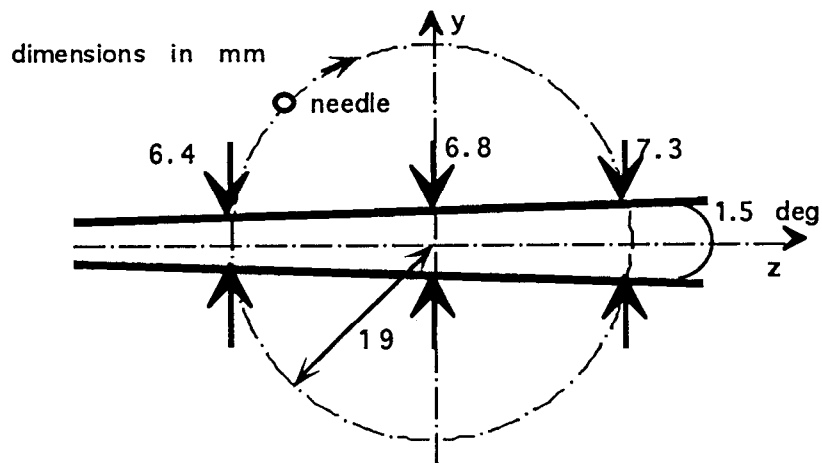


Fig. 9. Jet dimensions inside the Antiproton Accumulator: the 19 mm radius circle swept by the L-shaped needle when rotating around the x axis (notice the two intersections with the jet).

- *Cluster speed*

Another measurement needed for the evaluation of the cluster-jet density is the speed of the clusters. The literature [7, 8] states that this speed shows a distribution with a narrow peak around a well-defined value, thus, we can treat the clusters as all having the same velocity.

To make this measurement we periodically chopped the jet inside the Antiproton Accumulator pipe and looked downstream (in the R1 chamber) for the propagation of this perturbation, thus measuring the elapsed time. The chopper consisted of a rotating metal cylinder with two "quarter period" windows (fig.10) with its axis along the  $x$  direction. Its motor allowed rotation frequencies as high as 400 Hz. The detector was an ion gauge installed in R1 and positioned on the jet stream line. The time response of the electronics was of the order of  $\mu\text{sec}$  compared to a flight-time of almost a millisecond.

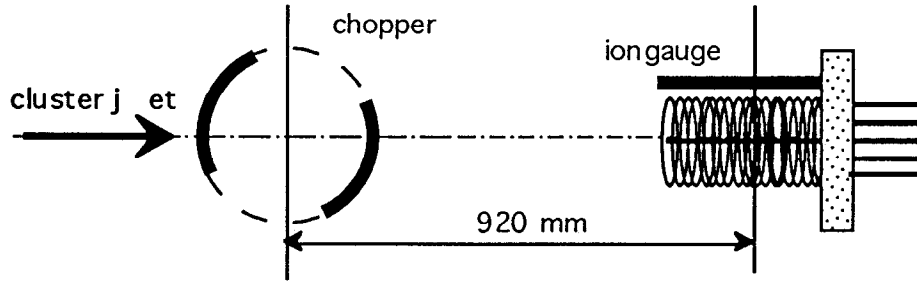


Fig. 10. Set-up for the cluster speed measurement: the chopper is inside Antiproton Accumulator and the detector (a common ion gauge) is inside R1.

We measured the phase difference between the chopper and the signal of the ion gauge with a lock-in amplifier. The trigger comes from a thin slit on the cylinder that periodically passes between a LED and a photo transistor. We have the relation:

$$\Delta\phi = 360 \cdot (2f)t_{of} + c, \quad (4)$$

where  $\Delta\phi$  is the phase difference between the ion-gauge signal and the chopper,  $2f$  is the chopping frequency (twice the motor rotation frequency),  $t_{of}$  is the *time of flight*, and  $c$  a constant (frequency independent) offset. So, we have a linear relation between  $\Delta\phi$  and  $f$  (fig.11) and, by repeating the measurement at different values of  $f$ , we can extract  $t_{of}$  as:

$$t_{of} = \frac{1}{2} \frac{1}{360} \frac{d(\Delta\phi)}{df}. \quad (5)$$

Knowing the distance between the chopper and detector (920 mm) we can obtain  $v_{cl}$ .

Using the same assumptions as in equation (2) we obtain an expression for the speed of the clusters:

$$v = \sqrt{\frac{2R}{W} \left( \frac{\gamma}{\gamma-1} \right) T_0}. \quad (6)$$

Note that (6) is independent of stagnation pressure and nozzle geometry and does not consider any condensation process effects. For  $T_0=77$  K,  $\gamma=5/3$  from (6) we have  $v = 1260$  m/s. The values

measured for  $v_{cl}$  are shown in fig.12. At low pressure, (J1 pressure less than  $10^{-2}$  torr) the measured value is about 1200 m/sec, in good agreement with the prediction.

Figure 12 also shows the RMS value of the ion gauge signal (the so called chopped jet signal ). Notice that the rms value of the ion gauge signal has the same shape as the cluster-jet throughput shown in fig.6b. Both the approximately linear rise at low pressure and the fall off to near zero at high pressure seen in 6b are reproduced here. This confirms that the increase of the throughput in R1 at high hydrogen line pressure (fig.6a), is due to gas diffusion, as previously discussed.

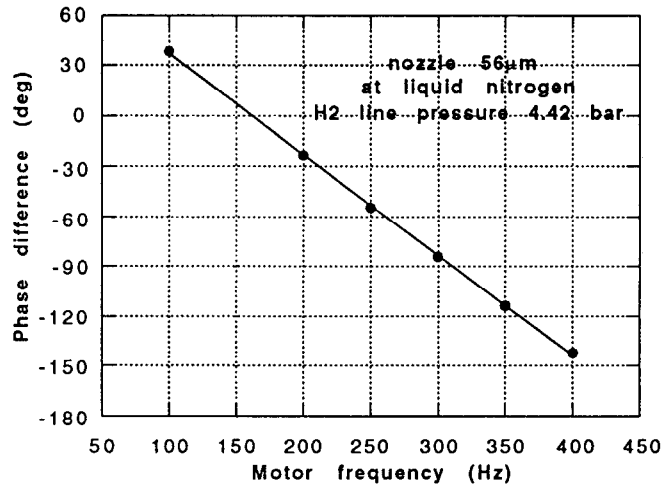


Fig. 11. Phase difference between ion gauge signal and LED/photo transistor signal, as a function of the chopper rotation frequency.

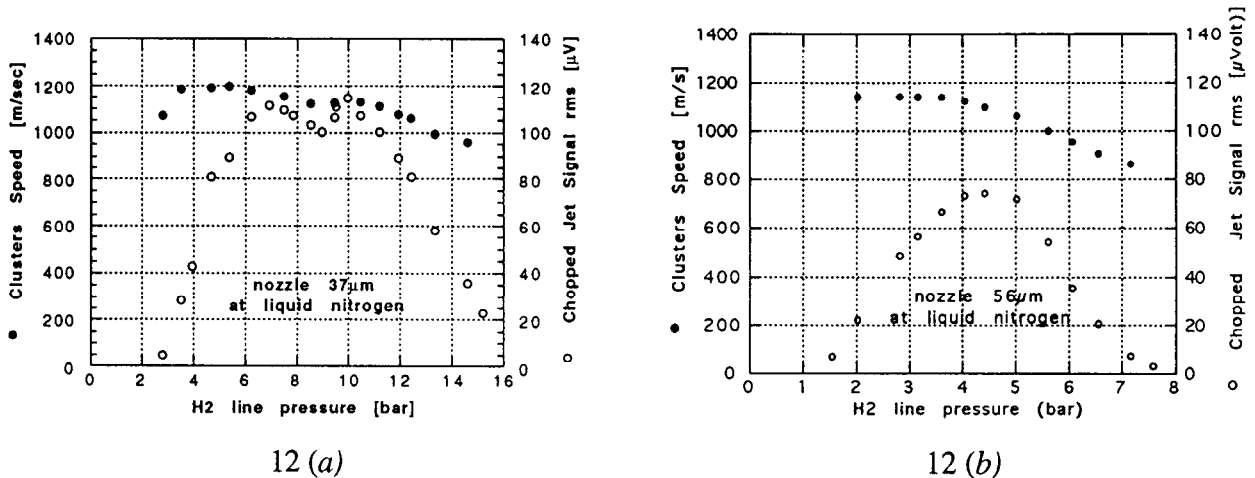


Fig. 12. Speed of the clusters and ion gauge signal : a) for the 37  $\mu$ m nozzle; b) for the 56  $\mu$ m nozzle.

- *Results on Gas-jet Density*

Having determined the jet characteristics, we are able using equation (1) to evaluate the cluster-jet average density. Since the cluster velocity and the jet cross-section have been found to be independent of pressure, the density plot (fig. 13) has essentially the same shape as the the cluster-jet throughput in fig. 6b ( $v_{cl}$  varies little in that pressure range).

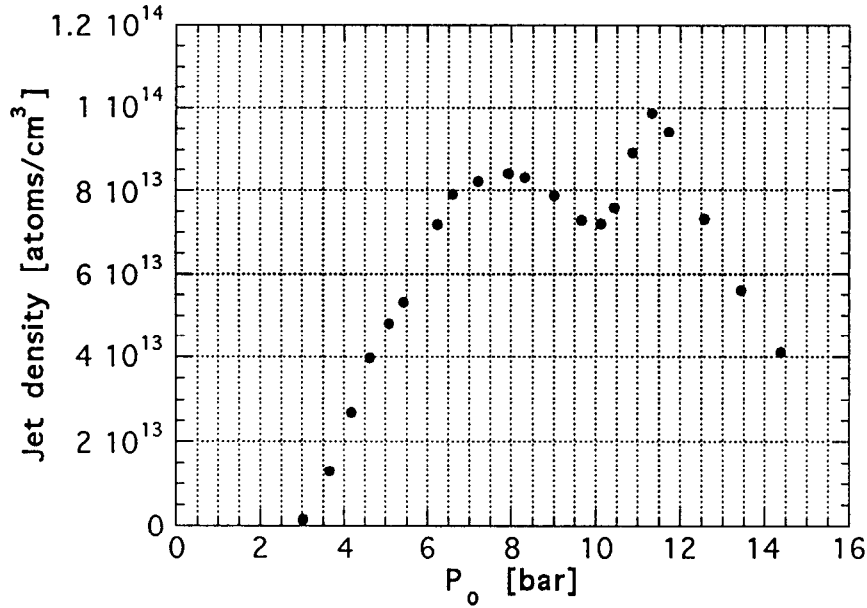


Fig. 13. Density of the cluster-jet as function of H<sub>2</sub> pressure.

- *Suggestions for Optimizing Gas-jet Performance*

Optimizing the gas-jet performance involves a balance between maximizing the cluster-jet density and minimizing the amount of background gas which enters the Antiproton Accumulator. The behavior seen in fig 6b strongly suggests that one operate in the linear region below or near the maximum throughput. As discussed, the extent of this region is set by the requirement that the pressure in J1 be below 10<sup>-2</sup> torr. Given the pumping speed of the J1 chamber, the nozzle flow is limited to about 8 · 10<sup>20</sup> atoms / s. This means we must choose our working point ( $P_0, T_0$ ) below the appropriate constant flow line for different nozzle sizes as shown in fig.14.

For a stagnation temperature  $T_0$  below the hydrogen critical point we have another constraint: to keep hydrogen in the gaseous phase the working point must be on the right side of the phase transition curve in fig.14.

To determine the conditions for maximum jet cluster density, we first introduce the parameter

$$\alpha(p_0, T_0) = \frac{\dot{m}}{\Phi_{jet}}, \quad (7)$$

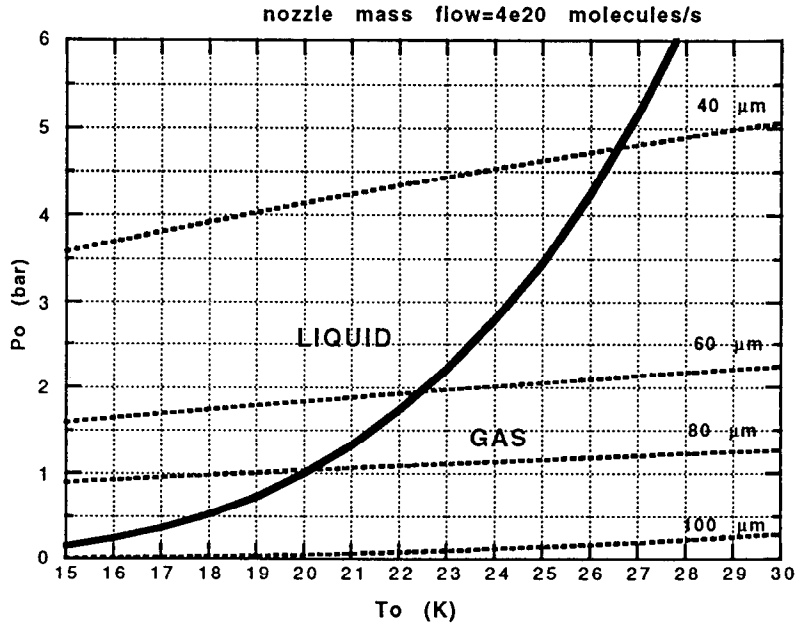


Fig. 14. Phase transition curve (solid line) for hydrogen and constant-nozzle mass flow (dashed lines) for four nozzle throat diameters. The hydrogen critical point is ( $P_0=13$  bar,  $T_0=33$  K). The flow lines are given by equation (2).

i.e. the ratio of the total mass flux through the nozzle to the cluster-jet flux. Next we note that, if we keep  $\dot{m}$  fixed, eq. (2) relates  $P_0$  to  $T_0$ , so that  $\alpha$  can be thought of as a function of  $T_0$  only. Now from (1), (6) and (7) we get

$$\bar{\rho}_{jet} \propto \frac{\alpha(T_0)}{\sqrt{T_0}} \quad (8)$$

since the process of clustering and formation of the jet is related to a sudden decrease in temperature, we can argue that it does not get worse as  $T_0$  is brought down, i.e. that  $\alpha$  is a non-increasing function of  $T_0$ . Eq; (8) then states that the jet density grows at least as the inverse square root of  $T_0$ . This implies that the best working condition (highest cluster-jet density) is at the lowest temperature attainable by the cryocooler and, consequently, that the nozzle throat diameter must be chosen in order to work with the maximum nozzle mass flow (i.e.  $4 \cdot 10^{20}$  molecules/s, with the present J1 pumping speed) at this temperature. If, for example, the lowest temperature is 20K then the nozzle throat should have a diameter of 80  $\mu\text{m}$  or larger (fig.14) (the nozzle throat diameters commonly used [9] are not larger than 140  $\mu\text{m}$ ). If we use a nozzle with a diameter smaller than 80  $\mu\text{m}$ , this simple theory tells us that the best working condition is at the intersection of the constant flow line for the particular size nozzle and the phase transition curve, so the nozzle temperature should be higher.

In practice, we plan to determine the best cluster-jet density conditions ( $P_0$ ,  $T_0$  and  $d$ ) in the fall of 1994 when the cryocooler has been installed and the modifications to the J1 chamber will have been

made. What we could already note is that, at  $T_0=77$  K, our measurements show a higher value for the maximum cluster-jet throughput for the  $37\ \mu\text{m}$  nozzle than for the  $56\ \mu\text{m}$  one, as can be argued from figs. (6a), (6b). This may be due to the effect of a higher pressure (with the same nozzle mass flow) on the clusterization process for the  $37\ \mu\text{m}$  nozzle.

• *Reducing Background Gas in the Antiproton Accumulator*

Let us now consider the hydrogen molecules from the gas-jet that the antiproton beam sees outside the target region along its orbit in the antiproton accumulator. We measured a "background throughput" (as defined on page 4) inside the Antiproton Accumulator pipe of about  $10^{-3}$  torr-liter/sec with the  $37\ \mu\text{m}$  nozzle at 8 bar. Given this result and the evaluation of the pumping speed for each region of the antiproton accumulator beam pipe, in particular close to the jet target region, we can compare the number of atoms the beams sees outside and within the interaction region. The pumping speed of the TMPAA1 turbomolecular pump is 650 liters/sec as is that of the TMPAA2 pump (fig.2a), while that through the Antiproton Accumulator beam pipe is calculated to be about 100 liters/sec: this gives an overall pumping speed for this section of about 1400 liters/sec. The number of atoms per unit area (for the measured throughput of  $10^{-3}$  torr-liter/sec) the antiproton beam sees in this 2 meter region adjacent to the interaction area is therefore about  $10^{13}$  atoms/cm<sup>2</sup>. The gas leaving this section contributes to the number of atoms the beam sees along the rest of its orbit and is estimated to contribute an additional  $10^{13}$  atoms/cm<sup>2</sup>. The total thickness of the background gas is, therefore, about  $\frac{2}{3}$  that of the cluster-jet. Installing a getter pump, with a pumping speed higher than 1000 liter/sec, upstream of the jet target (due to the reduced diameter of the beam pipe, the conductance downstream of the target is small) could reduce the total thickness of the background gas by about 50%. This would then increase the beam lifetime by about 20%.

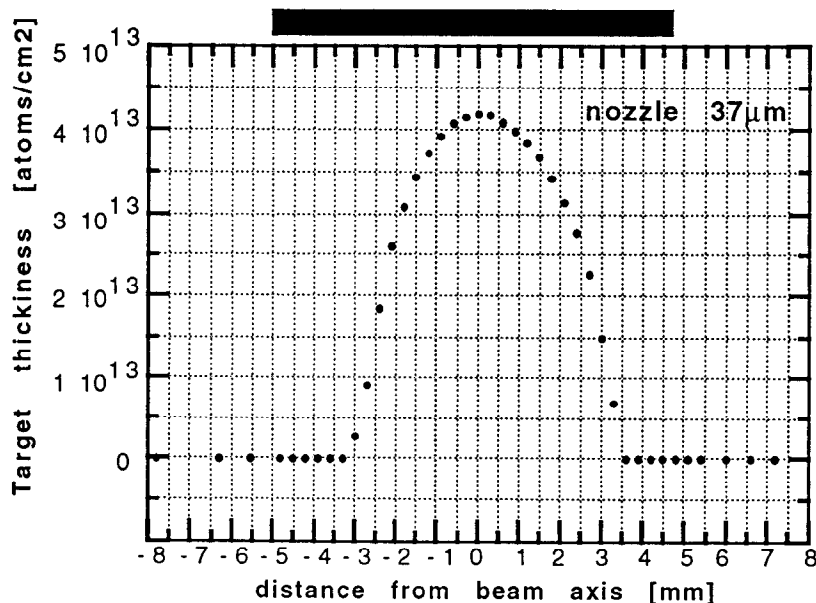


Fig.15. Jet target thickness in the interaction region.

It may be useful to define a quantity "jet target efficiency" *JTE* as the ratio between the cluster-jet target thickness and the total gas thickness (jet + background). This is plotted in fig. 16 for the 37  $\mu\text{m}$  nozzle, together with the density plot. As would be expected, the highest efficiency does not coincide with the highest jet density. This suggests that, in order to have the highest integrated luminosity, the best working point is somewhat below the highest achievable density.

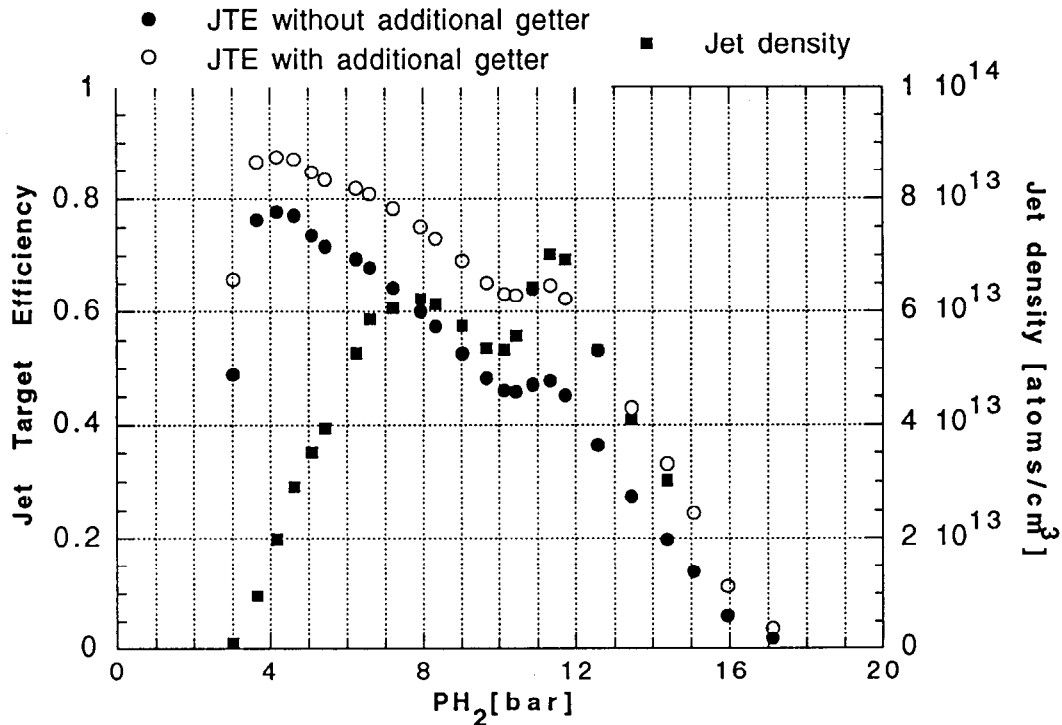


Fig.16. The cluster-jet average density calculated from (1) for the 37  $\mu\text{m}$  nozzle (for the 56  $\mu\text{m}$  we get a maximum density of about  $4.5 \cdot 10^{13}$  atoms/cm<sup>3</sup> at 4.5 bar) and the Jet Target Efficiency with the same nozzle. Black points refer to the present configuration of the pumping system while white points are an estimate of what we would get by adding a getter pump in the Antiproton Accumulator pipe upstream of the jet, as we suggest in the text.

Finally we want to note that we have the possibility of keeping the luminosity constant during the run time of the experiment. This is possible by monitoring the rate of events (with the *luminosity monitor*) and adjusting the  $\text{H}_2$  line pressure accordingly. As the antiproton beam intensity decreases, one may gradually raise the pressure and thus the cluster-jet density

#### • Acknowledgements

This work was made possible thanks to the help and support of J. Barilla, R. Davis, D. Miller, M. Urso and the entire technical staff at the Proton Assembly Building. We also thank Genoa I.N.F.N. technicians who worked for the construction and set-up of the E760 Jet Target: D. Bondi, E. Bozzo, F. Conforti, R. Cereseto, G. Franzone, A. Manco, G. Massari, M. Negri, A. Pozzo. We are grateful to Prof. R. Mattera for the useful discussions in that phase and during tests preparation. Finally, thank you to S. Pordes for critically reviewing this paper.

Pumping Speed for N <sub>2</sub>	Pumping Speed for H <sub>2</sub>	Conductance for H <sub>2</sub>
$S_{J1} = 1180$ lit/sec	$S_{J1} = 1450$ lit/sec	
	$S_{J2} = 650$ lit/sec	$C_{J1-J2} = 2$ lit/sec
$S_{J3} = 480$ lit/sec	$S_{J3} = 660$ lit/sec	$C_{J2-J3} = 6$ lit/sec
$S_{AA} = 115$ lit/sec	$S_{AA} = 430$ lit/sec	$C_{J3-AA} = 25$ lit/sec
$S_{AA1} = 520$ lit/sec	$S_{R3} = 700$ lit/sec	$C_{AA-R3} = 40$ lit/sec
	$S_{R2} = 740$ lit/sec	$C_{R3-R2} = 100$ lit/sec
$S_{R1} = 1130$ lit/sec	$S_{R1} = 2350$ lit/sec	$C_{R2-R1} = 150$ lit/sec

Tab.1. Measured values of the pumping speed (N<sub>2</sub> and H<sub>2</sub>) and conductance (H<sub>2</sub>). These pumping speeds are measured for pressures below  $5 \cdot 10^{-4}$  torr. The AA pumping speed during the test was limited by the system used for the cluster-jet shape measurements.

• **References**

- [1] T.A. Armstrong et al., *Phys. Rev. Lett.* , **68**, 1468 (1992)
- [2] T.A. Armstrong et al., *Nucl. Phys.* , **35 B**, 373 (1992)
- [3] T.A. Armstrong et al., *Proposal to continue the study of charmonium spectroscopy in proton-antiproton annihilation*, Fermilab proposal 835, (1992).
- [4] G. Boero, *graduation thesis* , University of Genoa, Italy (1994)
- [5] D.R. Miller, *Free jet sources* (vol.1, pag.14-53 of *Atomic and molecular beams methods*, G.Scoles ed., Oxford Univ. Press, 1988)
- [6] M.Kappes and S.Leutwyler, *Molecular beams of clusters* (vol.1, pag.380-415 of *Atomic and molecular beams methods*, G.Scoles ed., Oxford Univ. Press, 1988)
- [7] O. F. Hagen, W. Obert, *J. Chem. Phys.*, **56**, 1793 (1972)
- [8] J.Gspann and K.Korting, *J. Chem. Phys.*, **59**, 4726 (1973)
- [9] W.Obert, *Cluster beams formed with supersonic nozzle*, Proc.11th symp. on rarefied gas dynamics, Cannes (1978)